Les Cahiers du GERAD ISSN: 0711–2440

Testing geological heterogeneity representations for enhanced oil recovery techniques

E. Tamayo-Mas, H. Mustapha, R. Dimitrakopoulos

G–2016–108

November 2016

GERAD HEC Montréal
3000, chemin de la Côte-Sainte-Catherine
Montréal (Québec) Canada H3T 2A7

Tél. : 514 340-6053
Téléc. : 514 340-5665
info@gerad.ca
www.gerad.ca

Testing geological heterogeneity representations for enhanced oil recovery techniques

Elena Tamayo-Mas [a]

Hussein Mustapha [b]

Roussos Dimitrakopoulos [a, c]

[a] *COSMO – Stochastic Mine Planning Laboratory, Department of Mining and Materials Engineering, McGill University, Montréal (Québec), Canada, H3A 2A7*

[b] *Schlumberger. Abingdon Technology Centre, Lambourn Court, Wyndyke Furlong, Abingdon, OX141UJ, United Kingdom*

[d] *GERAD, HEC Montréal, Montréal (Québec), Canada, H3T 2A7*

elena.tamayomas@mcgill.ca
hmustapha@slb.com
roussos.dimitrakopoulos@mcgill.ca

November 2016

Les Cahiers du GERAD

G–2016–108

Abstract: This paper analyzes the effects of geological heterogeneity representation in a producing reservoir, when different stochastic simulation methods are used, so as to assess the consequent effects on flow responses for different Enhanced Oil Recovery (EOR) techniques employed. First, the spatial heterogeneity of a fluvial reservoir is simulated using three different stochastic methods: 1) the well-known two-point sequential Gaussian simulation (SGS), 2) a multiple-point filter-based algorithm (FILTERSIM), and 3) a new alternative high-order simulation method that uses high-order spatial statistics (HOSIM). Numerical results show that SGS suffers from the inability of describing the highly permeable channel network whereas FILTERSIM better reproduces this connectivity. By means of the recent HOSIM, a more appropriate description of the curvilinear high-permeability channels is obtained. Second, the realizations generated above represent permeability fields in EOR numerical simulations. In particular, four different methods are considered, namely: 1) surfactant, 2) polymer, 3) alkaline-surfactant-polymer and 4) foam flooding processes. The numerical results show that properly reproducing the main geological features of the reference images has a higher impact if surfactant or alkaline chemicals are injected rather than polymer or foam. This is due to the fact that these latter chemicals act by mitigating the effects of heterogeneities.

Keywords: Enhanced oil recovery, geologic heterogeneity, geostatistical algorithms, connectivity

1 Introduction

Conventional primary and secondary oil production techniques typically recover between 20% and 40% of the oil in place in an oil field (Muggeridge et al. 2014). To increase this oil recovery factor, tertiary or Enhanced Oil Recovery (EOR) techniques may be applied. Although the application of these EOR projects strongly depends on the economics and oil prices (see e.g. Alvarado and Manrique (2010)), these methods are seen as effective methods to improve recovery factors in reservoirs in the near future. As stated in the review by Sandrea and Sandrea (2007), the sweep and displacement efficiencies can be improved, thus achieving an additional 7-15% in oil recovery after water flooding, if tertiary oil recoveries are implemented.

Chemical EOR techniques have recently drawn increasing interest. After sweeping the reservoir with water flooding, some oil is still left behind in small pores, which may be displaced if the high capillary pressure is overcome. Surfactant flooding, Schramm (2000), works in this direction: by adding a small amount of surfactant into the injected fluid stream, the oil/water interfacial tension is lowered. Thus, additional oil may be displaced by water. Another way to achieve favourable oil recovery is by adding polymer, Shah (2012), in the injected water. The main objective of this method, the so-called polymer flooding, is, firstly, to make the injected solution more viscous (while that for the oil remains unaltered) and secondly, to reduce the rock permeability to water (thus unaffecting the permeability to oil). As a consequence, the mobility of the polymer solution is then lower than that of pure water, whereas that for the oil remains unaltered, thus improving the sweep efficiency of the flooding. The effectiveness of these two EOR techniques is hampered by the tendency of the surfactant and the polymer to be adsorbed by the rock: if the adsorption is too high, large quantities of these chemicals may be required to produce small quantities of additional oil. This adsorption is reduced if surfactant and polymer are injected in conjunction with alkaline, Castor et al. (1981), chemicals (ASP flooding). Apart from reducing this rock adsorption, by adding these alkalines and letting them react with the petroleum acids, in-situ surfactants are formed. Hence, the oil/water interfacial tension is reduced and the rock wettability is changed, thus easily releasing the oil from the reservoir towards the production wells. Foam flooding, Fisher et al. (1990), may also be used to improve oil recovery. In gas or water-alternating-gas (WAG) injection techniques, the high mobility of the gas leads the oil to flow through high-permeable channels thus reducing the sweep efficiency. If foam is injected, the gas mobility is reduced thus increasing the effective viscosity and decreasing the relative permeability of the gas. Nevertheless, in spite of their relative simplicity and promising potential, EOR techniques are being slowly implemented, IEA (2013). This is due to the fact that these techniques are often expensive and difficult to be performed, since large quantities of chemicals and/or solvents are required. Hence, before the application of the most suitable EOR technique, its performance needs to be carefully analyzed.

One of the main challenges when assessing the recovery performance of EOR strategies is accounting for the risk associated with technological, economic and geological uncertainties. These concerns were already highlighted some decades ago by Brown and Smith (1984), who used Monte Carlo simulations to assess the uncertainties in a surfactant process; Gittler and Krumrine (1985), who financially quantified the uncertainties associated with various chemical EOR methodologies; Langtangen (1991), who analyzed the impact of uncertainty in some input parameters for a one-dimensional polymer flooding model; Bu and Aanonsen (1991), who dealt with surfactant flooding and Ghori et al. (1992), who emphasized the importance of the determination of uncertainty when describing the reservoir properties in a polymer flooding design. Nevertheless, due to the complexity of these EOR techniques, further research is still needed in this direction. As exposed by the recent contributions of Carrero et al. (2007), Mollaei et al. (2011), Othman et al. (2013), Alkhatib and King (2014), AlSofi and Blunt (2014) and Choudhary et al. (2014), a better understanding of the effect of parametric uncertainty, such as the chemical adsorption on rock surface, the interfacial tension and the residual oil saturation reduction by the chemical, is still required. In addition, the recent studies of Costa and Schiozer (2008), Alusta et al. (2012) and Galard et al. (2012) illustrate the importance of addressing economic uncertainty such as oil or chemical prices whereas the works of Delshad et al. (2009), Alajmi et al. (2010) and Kianinejada et al. (2013) show the influence of uncertainty derived from fracture's geometrical properties in case of applying surfactant or polymer floods in naturally fractured reservoirs.

As reviewed by Deutsch and Hewett (1996) for reservoir forecasting in general and highlighted in some recent works dealing with chemical and miscible flooding (Mantilla and Srinivasan (2011), Nguyen et al. (2014), Dang et al. (2014), Yu et al. (2013) and Alkhatib (2014)), accounting for the geological uncertainty that characterizes the rock properties in the subsurface needs a special consideration, since the spatial distribution of subsurface properties such as rock permeability and porosity fully affects groundwater flow responses. Due to their complexity and the sparsely

sampled data, geostatistical simulation methods have been proposed and have been thoroughly analyzed during the last decades, including the works by Journel (1989), Goovaerts (1997), Pyrcz and Deutsch (2014) and references therein.

Traditionally, variogram-based models that are conditioned only on second-order spatial statistics such as the sequential Gaussian simulation (SGS, Journel (1994)) and the sequential indicator simulation (SISIM, Journel and Alabert (1988)) have been used (Goovaerts (1997) and Deutsch and Journel (1998)). As detailedly discussed by Dimitrakopoulos and Luo (2004), the aim of the SGS is to decompose the multivariate probability density function of a stationary Gaussian random process into a product of univariate posterior distribution functions, where the posterior mean and variance are estimated by means of a simple kriging. Then, at each grid point, the realization is generated by randomly sampling from this posterior distribution. In spite of their good performance describing Gaussian processes, their robustness and their ease of conditioning, these variogram-based methods suffer from an inability of reproducing curvilinear geological patterns, since they only rely on two-point statistic. These shortcomings were first highlighted by Guardiano and Srivastava (1993) who set the basis of the multiple-point simulation algorithms. In contrast to the traditional variogram-based techniques, this new kind of geostatistical methods does not need the explicit definition of a random function since the required spatial information is directly inferred from conceptual geological models. Different multiple-point algorithms such as the single normal equation simulation (SNESIM) of Strebelle (2002) and recently improved by Strebelle and Cavelius (2014), the patch-based SIMPAT proposed by Arpat (2004), the filter-based FILTERSIM proposed by Zhang et al. (2006) and then expanded by Wu et al. (2008), the list approach technique (IMPALA) developed by Straubhaar et al. (2011) and then used as a basis by Comunian et al. (2012) for their novel approach, the distance-based non-stationary model by Honarkhah and Caers (2012) and the pattern-based CDFSIM developed by Mustapha et al. (2014) have been proposed in the literature (for a general overview we refer to the review by Hu and Chugunova (2008) and the recent contribution by Mariethoz and Lefebvre (2014)). FILTERSIM is very convenient from a computational viewpoint, since it employs a set of filters to scan the reference images and classify the patterns in a filter score space of reduced dimension: similar patterns are grouped together into a cluster, which is represented by a pattern prototype. During the simulation, a random path visiting all the grid points on which values are to be simulated is defined. Then, at each location, FILTERSIM determines the prototype closest to the conditioning data event (either original hard data or previously simulated values), randomly draws a pattern from this prototype and pastes it to the realization being simulated thus freezing the nodes within a central patch. However, these methods pose some drawbacks. For instance, multiple-point algorithms rely on the chosen reference image, which is a subjective conceptual model, and as a result, the information inferred from it may be misleading. To overcome this limitation, different new algorithms such as the high-order simulation algorithm (HOSIM) have been suggested. In HOSIM, Mustapha and Dimitrakopoulos (2010), the reference image and available data are first scanned to compute the so-called high-order spatial cumulants, see Dimitrakopoulos et al. (2010) for a detailed description of them. Then, a random path visiting all the grid points on which values are to be simulated is defined. Sequentially, for each node along this path, HOSIM defines a template within which the available conditioning data is searched. Then, the computed high-order spatial cumulants are used to define the coefficients of the Legendre series, which are employed to build the conditional probability density function (cpdf), see Mustapha and Dimitrakopoulos (2011) for a detailed description of the equations. Finally, a uniform random value is drawn from this distribution function and assigned to the node under consideration.

This paper addresses the effect of these different simulation algorithms on the spatial distribution of permeability and consequent flow responses when EOR techniques are taken into account. In particular, four different chemical methods (surfactant, polymer, alkaline-surfactant-polymer and foam flooding processes) are analyzed. The aim of this study is twofold. First, a comparative study of stochastic methods to account for geological heterogeneity is presented. Traditional and well-known algorithms (SGS and FILTERSIM) are here compared to the above mentioned new alternative high-order simulation method (HOSIM). Second, the effects of spatial variability of the permeability on the underground flows when chemical flooding processes are applied are investigated. The role of the high-permeability connectivity is here examined by means of this flow sensitivity analysis.

2 Geologic heterogeneity simulations

For the comparison study on the effect of spatial geologic heterogeneity and consequent flow responses when EOR techniques are considered, the three-dimensional permeability field of Figure 1(a) is used. The considered data set is one of the three layers in which the synthetic Stanford V reservoir (Mao and Journel 1999) is divided. This permeability field, described by means of 100x130x10 grid cells, is characterized by channels of different thicknesses and

orientations, see Figures 1(c)-1(e) for a detailed view of 2D-sections of the reservoir. Thus, the geological patterns to be reproduced are complex. All the stochastic algorithms are based on the same sparse data set, see Figure 1(b). Here, a data set of 50 values per layer are randomly sampled from the exhaustive image of Figure 1(a) (=0.38% of the reference image).

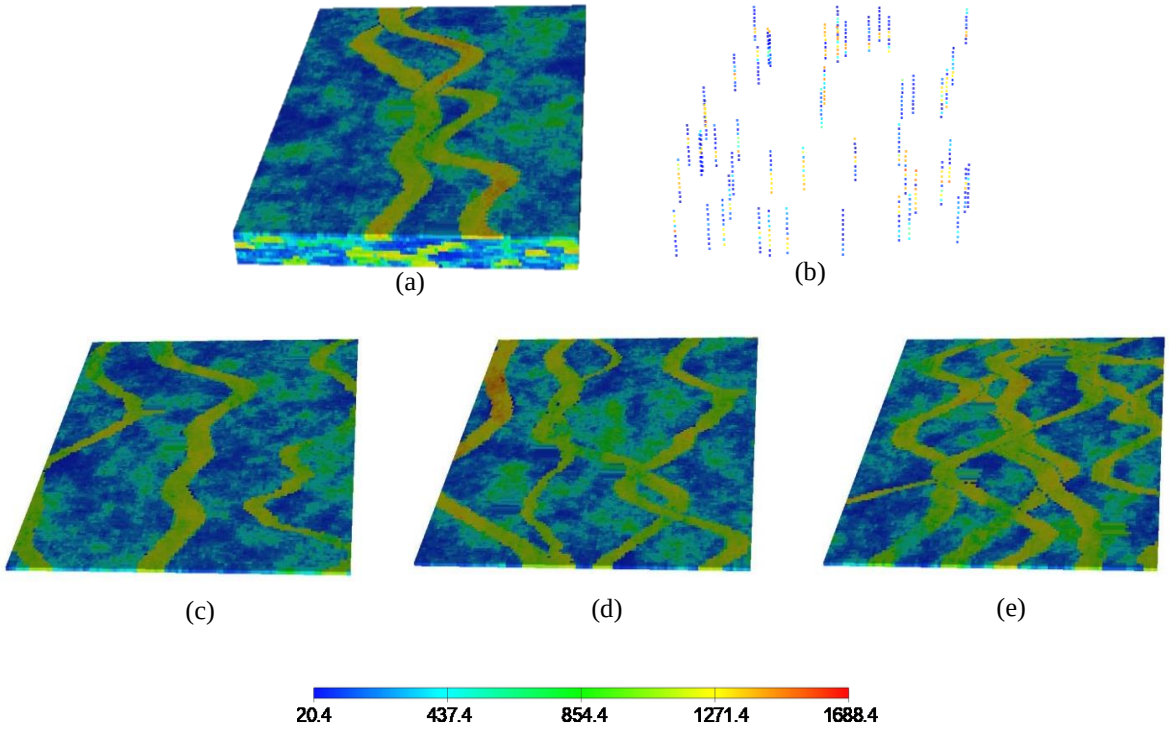

Figure 1: Three-dimensional permeability field used for our comparison study: (a) 3D reservoir (130000 points) used as a reference image; (b) a data set of 500 points randomly selected from (a) (=0.38% of the total number of points of (a)); (c)-(e) three 2D-sections of the reservoir.

Different realizations of the permeability field, see Figure 1(a), conditioned to the hard data of Figure 1(b) are generated using three of the aforementioned geostatistical models. Here all the simulations are done at a point scale. Then, these realizations are used as permeability fields in the flooding processes of Section 3.

First, the sequential Gaussian simulation method implemented in SGeMS (Remy et al. 2009) is used to generate ten different realizations; see three of them in Figures 2(a)-2(c). As seen, by means of this conventional algorithm the well-connected channels cannot be well reproduced. Second, the filter-based FILTERSIM continuous algorithm implemented in SGeMS is employed to simulated ten different realizations of the permeability field of Figure 1(a). In contrast to the traditional variogram-based technique, the spatial structure of channels is here better reproduced, see Figures 2(d)-2(f). To finish with, the new HOSIM method is used. Three of the obtained realizations can be seen in Figures 2(g)-2(i). Here, well-connected channels are obtained.

3 Enhanced oil recovery simulations

The effect of spatial heterogeneity on fluid flow behavior in case of EOR techniques is analyzed here by means of: 1) surfactant, 2) polymer, 3) alkaline-surfactant-polymer and 4) foam flooding processes. In these four models, the realizations generated above represent permeability fields in a 3D reservoir with an injector located at the top corner of the medium and a producer at the opposite bottom corner, see Figure 3. To discretize the reservoir, a regular grid of 130000 cells (100 x 130 x 10 grid cells) is used.

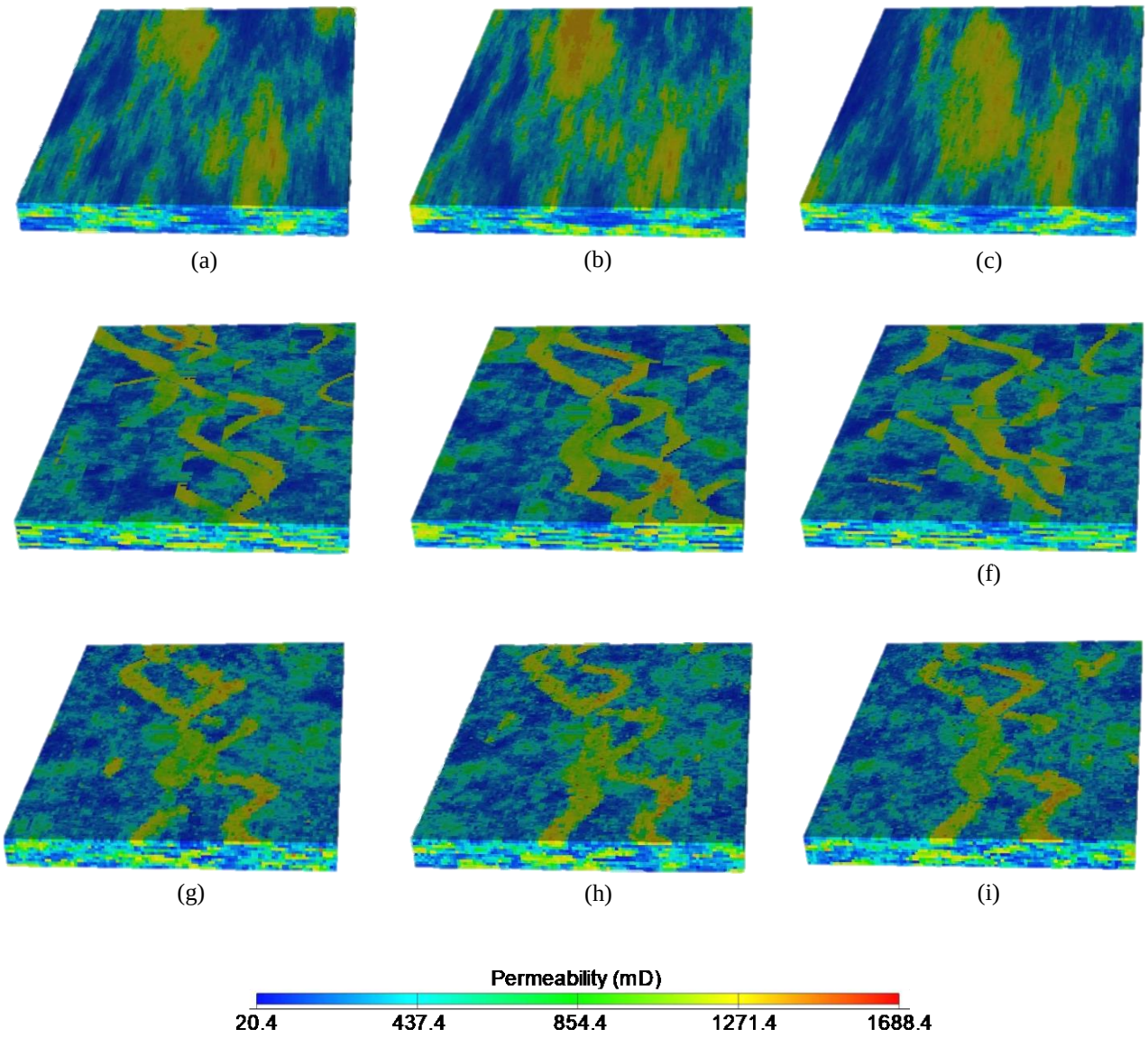

Figure 2: Three of the ten realizations generated by SGS (first row), FILTERSIM (second row) and HOSIM (third row) methods.

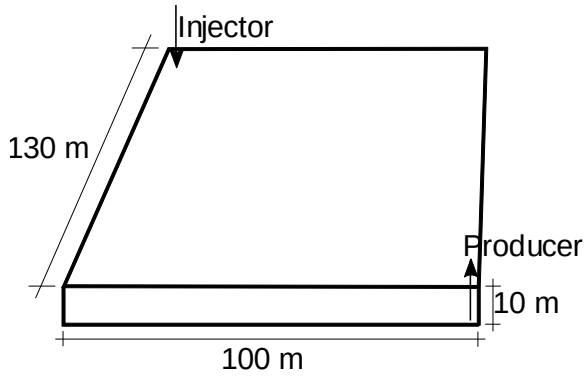

Figure 3: The domain geometry, injector and producer locations.

In each section, three different results are compared. First, the oil saturation profiles at a representative time step for the reference image (Figure 1(a)) and for SGS, FILTERSIM and HOSIM realizations are displayed and compared. Second, the oil production versus time curves for the reference image and for the three aforementioned geostatistical methods are considered. Third, the cumulative oil productions at an arbitrary time step for the reference image and for each of the realizations are presented. All flow simulations in this study are conducted using the ECLIPSE®, Schlumberger (2014), reservoir simulation software.

3.1 Surfactant flooding

The effect of spatial heterogeneity is first analyzed in a surfactant flooding process. The 3D domain of Figure 3 is considered, with an initial oil saturation of 0.85. Here, first, water is injected for a period of 10 days. Then, for a period of 400 days, surfactant is added to the injected water at a concentration of 30 kg/m^3. Finally, only water is injected for a period of 500 days. The rate of injection during all the flooding process is such that the bottom hole pressure equals 600 bar.

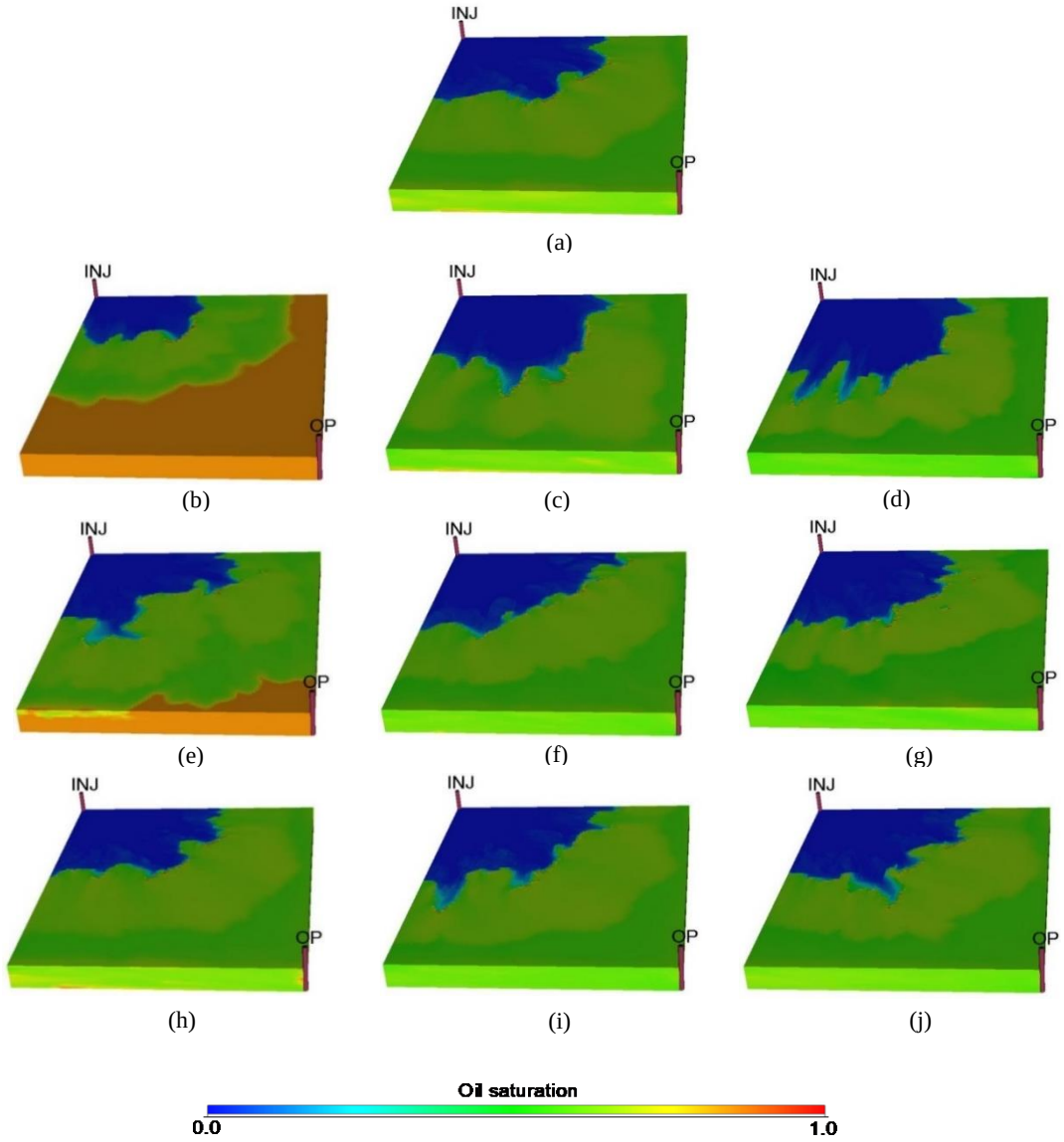

Figure 4: Surfactant flooding: oil saturation profiles at day 50 in the reference image (first row), SGS realizations (second row), FILTERSIM realizations (third row) and HOSIM realizations (fourth row). Note that in these last three rows, the oil saturation profiles corresponding to the lowest oil recovery (first column), a medium oil recovery (second column) and the highest low recovery (third column) have been selected.

The oil saturation profiles at day 50 are shown in Figure 4. If the permeability fields generated by the SGS algorithm are considered, significant differences in the flow behavior from one realization to another and with respect to the reference image are obtained, see Figures 4(b)-4(d). This is due to the fact that the SGS method does not reproduce well-connected channels of high-permeability. If FILTERSIM realizations are employed, the differences between the profiles are reduced. On the contrary, if HOSIM realizations are considered, approximately similar saturation profiles are obtained, see Figures 4(e)-4(j). This is because of the ability of these two methods to preserve connectivity in low- and high-permeability zones thus allowing the uniform propagation in the oil saturation profile.

Figures 5 to 7 display the cumulative oil production versus time curves when the reference image and the different realizations are used as permeability fields for the first 500 days of flooding. As seen in Figure 5, SGS results (dashed curves) are not in good agreement with the reference result (solid line) whereas Figure 6 shows a good agreement between FILTERSIM results (dotted curves) and the reference curve. As shown in Figure 7, this agreement is even better if HOSIM (dash-dot curves) realizations are employed.

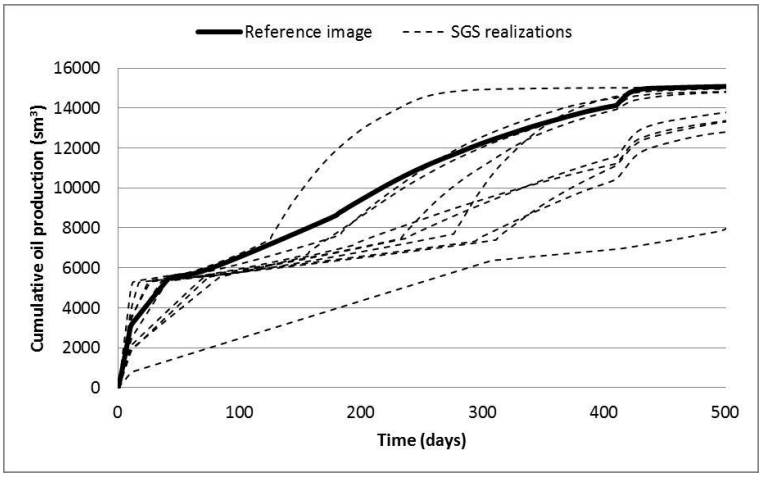

Figure 5: Oil production versus time curves for the reference image (solid line) and the SGS (dashed lines) realizations in case of surfactant flooding.

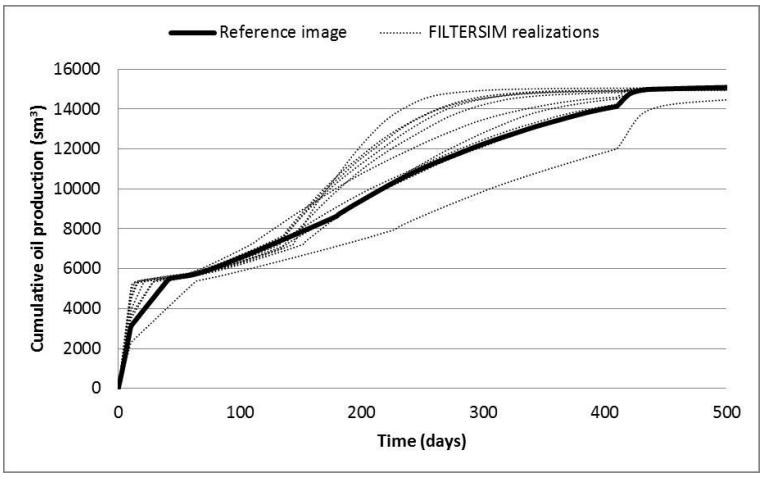

Figure 6: Oil production versus time curves for the reference image (solid line) and the FILTERSIM (dotted lines) realizations in case of surfactant flooding.

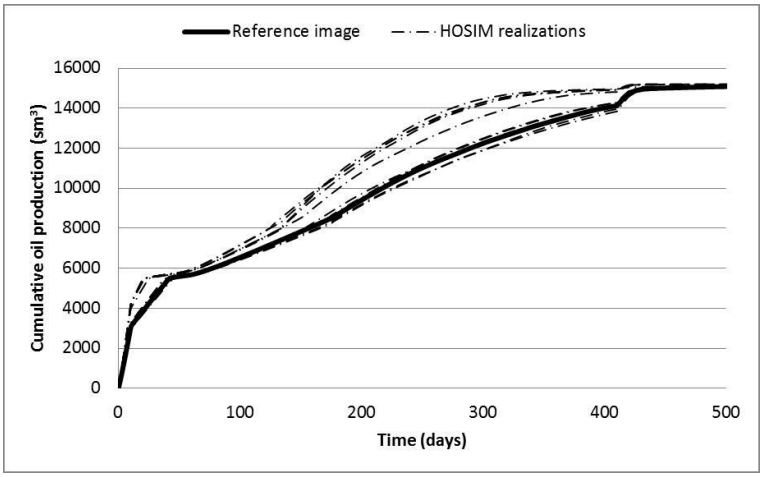

Figure 7: Oil production versus time curves for the reference image (solid line) and the HOSIM (dash-dot lines) realizations in case of surfactant flooding.

Figures 8 and 9 summarize the cumulative oil production obtained for each realization after the arbitrarily selected 300 days and at the end of the flooding (after 910 days) respectively. In general, if SGS permeability fields are used, the oil recoveries are not accurately reproduced: after 300 days of flooding, the relative error of the oil recovery production with respect to the reference solution is around 18% whereas at the end of the flow simulation, this is around 6%. Oil produced when FILTERSIM and HOSIM realizations are used is more accurately reproduced. The relative error of the oil recovery obtained with FILTERSIM realizations with respect to the reference recovery is around 9% after 300 days of flooding and is around 1% at the end of the simulation whereas HOSIM realizations lead to an error of 7% and 0.07% respectively. This oil variation is lower due to the fact that FILTERSIM and HOSIM realizations present much better connected channels than SGS and the connectivity is consistent with the reference image.

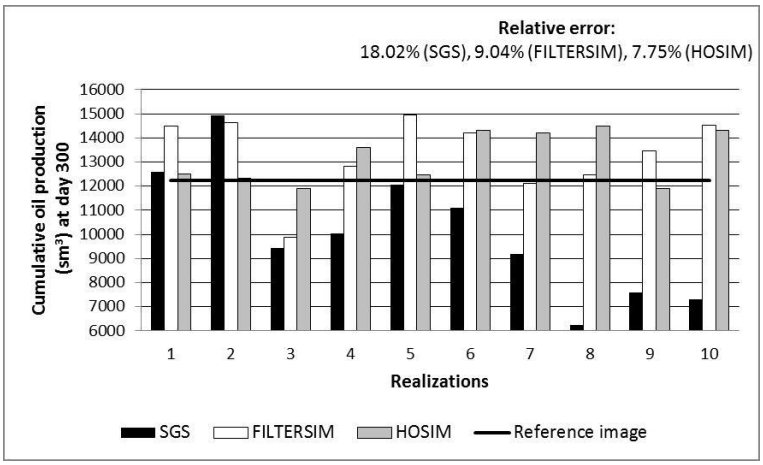

Figure 8: Cumulative oil production obtained for each realization after 300 days in case of surfactant flooding.

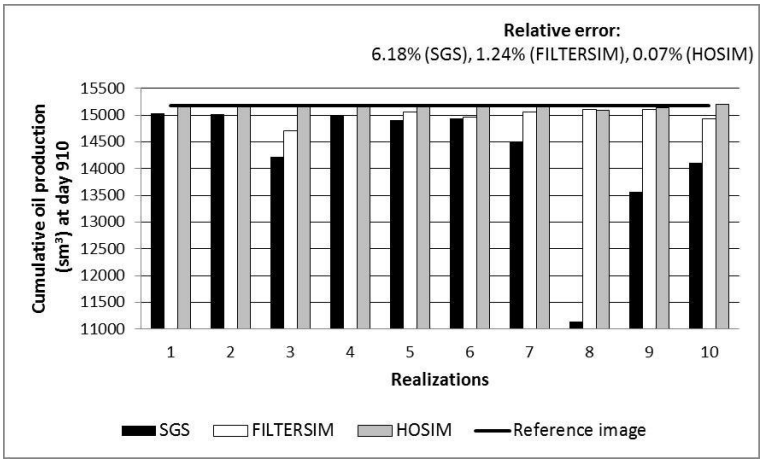

Figure 9: Cumulative oil production obtained for each realization after 910 days (at the end of the flow simulations) in case of surfactant flooding.

3.2 Polymer flooding

In the second test, a polymer flooding process is carried out. The 3D reservoir in Figure 3 with an initial oil saturation of 0.75 is considered. First, water (at a rate of 200 scm/day) and polymer are injected simultaneously for a period of 360 days. The concentration of polymer in this injection stream is 10.5 kg/sm^3. Then, for a period of 40 days, only water is injected.

The oil saturation profiles at day 50 are shown in Figure 10. As seen in this figure, small differences from one realization to another and with respect to the reference image are obtained. In contrast to surfactant flooding, the continuous and smooth propagation of the oil saturation profile (Figure 10(a)) is preserved if the SGS (Figures 10(b)-10(d)), FILTERSIM (Figures 10(e)-10(g)), and HOSIM (Figures 10(h)-10(j)) algorithms are employed.

Figures 11 to 13 show the oil production versus time curves when the reference image and the different stochastic methods are used to generate the permeability scenarios. As seen, an excellent agreement between all of them is observed, regardless of the method, see Figures 14 to 16 for a close-up view. Figures 17 and 18 confirm this behavior: after 50 days of flooding, the relative error of the oil recovery production with respect to the reference solution is around 1%, 0.07% and 0.02% if SGS, FILTERSIM and HOSIM permeability fields are used, respectively, whereas at the end of the flooding it is around 1%, 0.33% and 0.09% respectively. This little effect is due to the wettability of the reservoir, since the water-wet rock behavior makes the polymer solution not much effective.

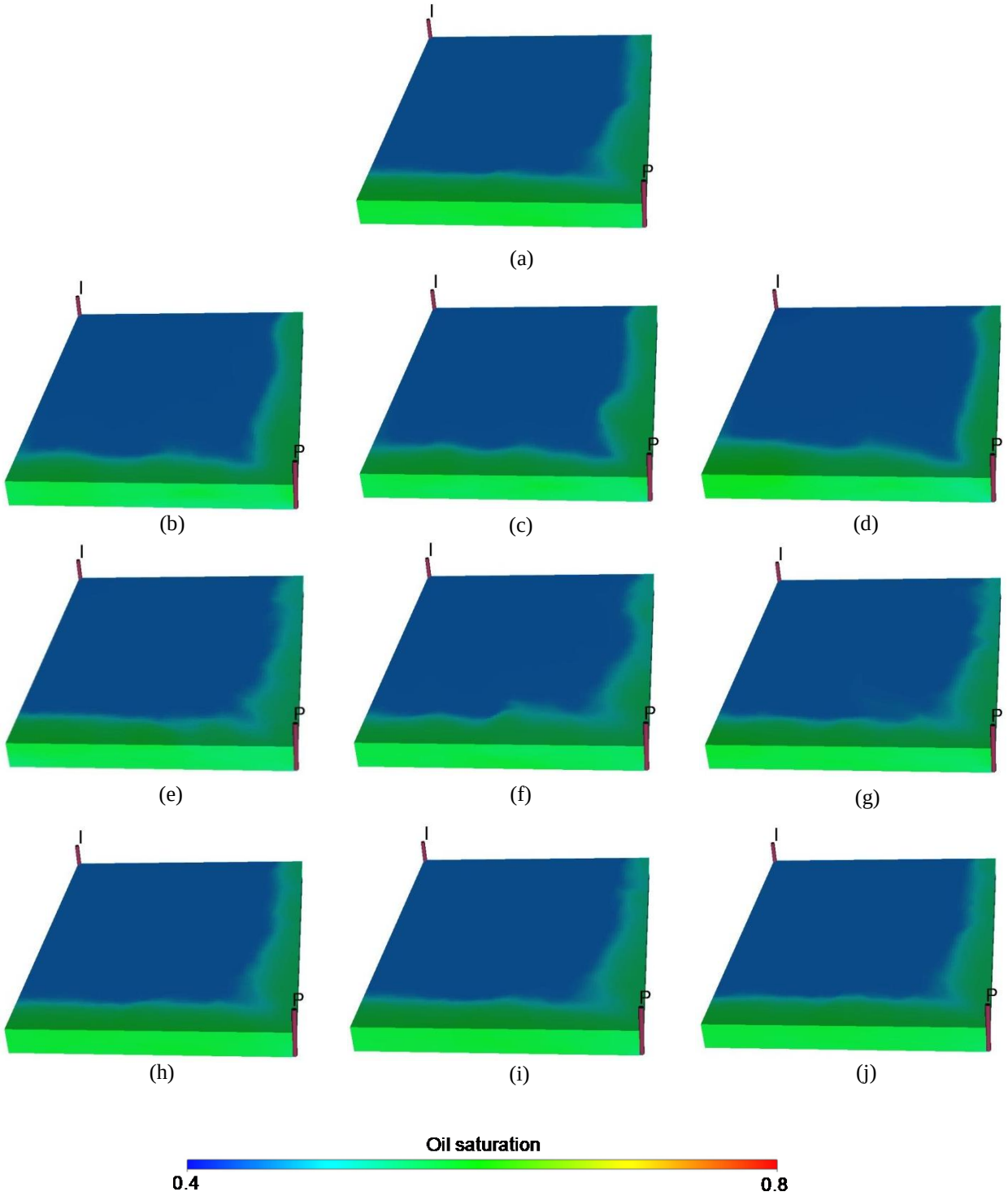

Figure 10: Polymer flooding: oil saturation profiles at day 50 in case of the reference image (first row), SGS realizations (second row), FILTERSIM realizations (third row) and HOSIM realizations (fourth row).

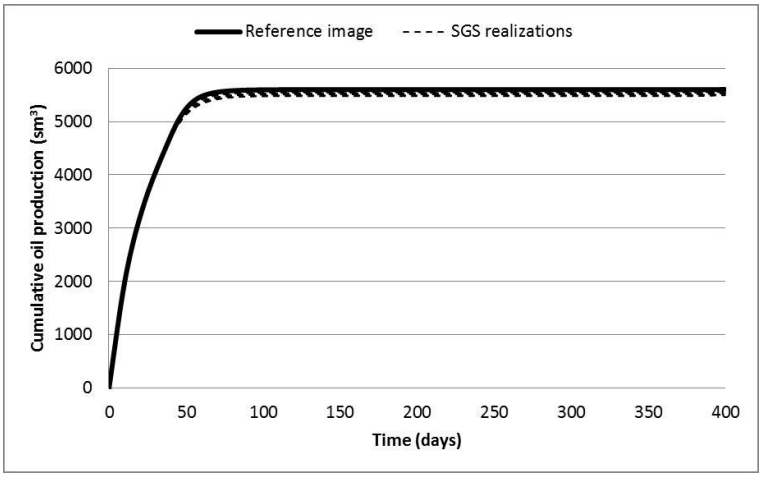

Figure 11: Oil production versus time curves for the reference image (solid line) and the SGS (dashed lines) realizations in case of polymer flooding.

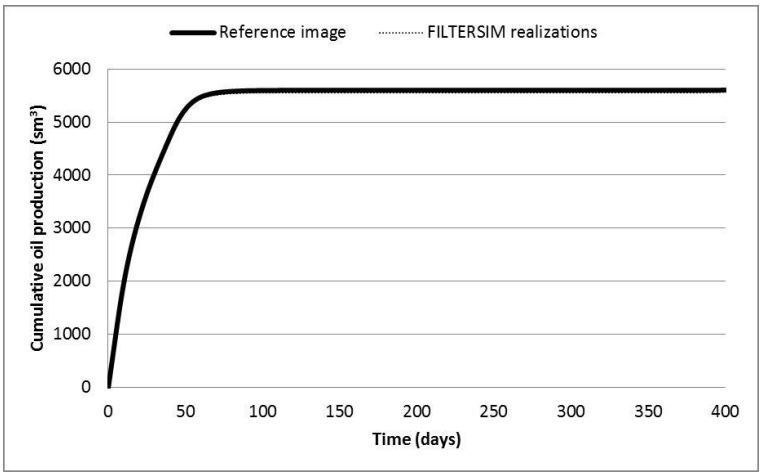

Figure 12: Oil production versus time curves for the reference image (solid line) and the FILTERSIM (dotted lines) realizations in case of polymer flooding.

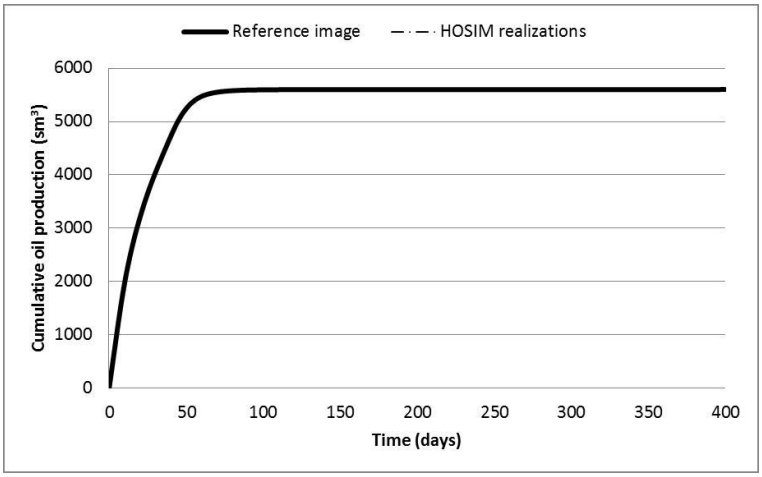

Figure 13: Oil production versus time curves for the reference image (solid line) and the HOSIM (dash-dot lines) realizations in case of polymer flooding.

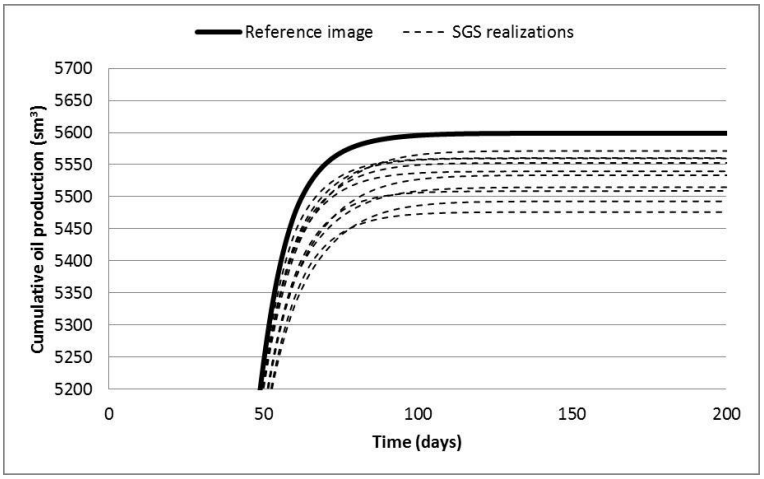

Figure 14: A close-up of the oil production versus time curves for the reference image (solid line) and the SGS (dashed lines) realizations in case of polymer flooding.

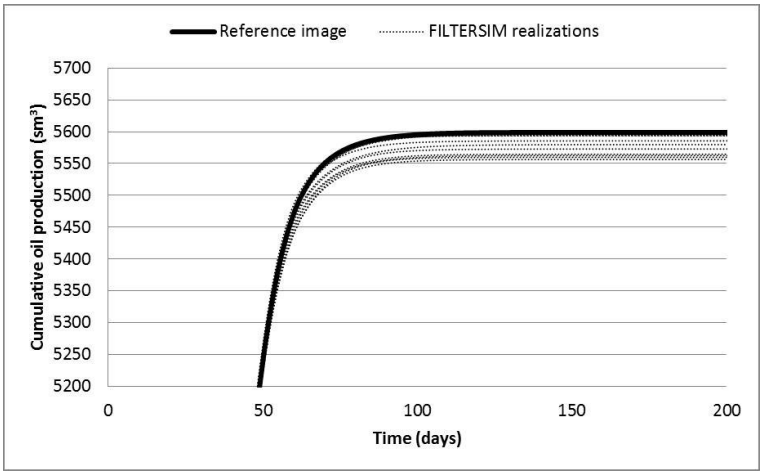

Figure 15: A close-up of the oil production versus time curves for the reference image (solid line) and the FILTERSIM (dotted lines) realizations in case of polymer flooding.

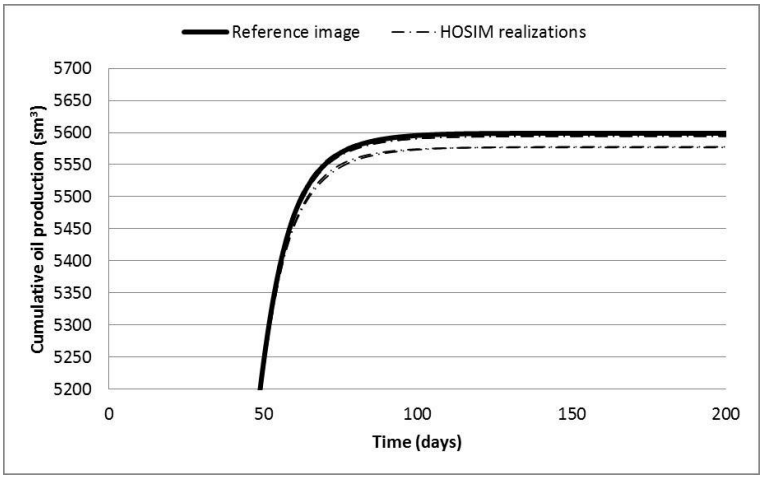

Figure 16: A close-up of the oil production versus time curves for the reference image (solid line) and the HOSIM (dash-dot lines) realizations in case of polymer flooding.

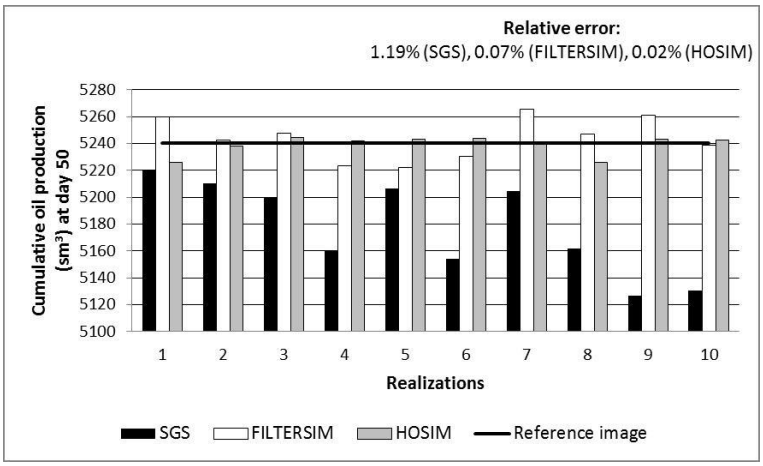

Figure 17: Cumulative oil production obtained for each realization after 50 days in case of polymer flooding.

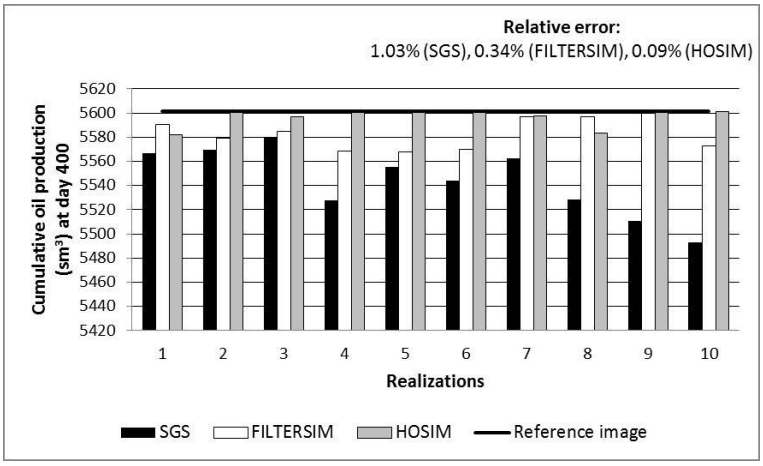

Figure 18: Cumulative oil production obtained for each realization after 400 days (at the end of the flow simulations) in case of polymer flooding.

3.3 ASP flooding

An alkaline-surfactant-polymer (ASP) flooding process is simulated in this section. The 3D reservoir of Figure 3 with an initial oil saturation of 0.45 is here considered. First, a mixture of alkaline, surfactant and polymer is injected for a period of 1000 days. The concentrations of these chemicals in the injection stream are 3.5, 10.5 and 10.5 kg/sm^3 respectively. Finally, only water is injected for a period of 500 days. The rate of injection during all the flooding process is such that the surface flow rate equals 200 sm^3/day or the bottom hole pressure for the injection well equals 7000 bar.

The oil saturation profiles at day 90 are shown in Figure 19. As discussed in Section 3.1 for the surfactant flooding, the continuous and smooth behavior of the permeability distribution of Figure 1(a) is not preserved if the SGS algorithm is employed. Thus, the uniform propagation of the oil saturation profile, see Figure 19(a), is not observed if SGS realizations are used as permeability fields, see Figures 19(b)-19(d). To the contrary, FILTERSIM realizations lead to a more uniform propagation of the oil saturation profile, Figures 19(e)-(g), since the generated high-permeability channels are better reproduced. When HOSIM permeability fields are used, the flow behavior is more uniform and few differences are observed from one realization to another and with respect to the reference image, as shown in Figures 19(h)-19(j).

The cumulative oil production is used here again to qualitatively and quantitatively assess the effect of the geologic heterogeneity. Figures 20 to 22 display the cumulative oil production versus time curves for the first 600 days of

flooding when the different stochastic methods are used to generate the permeability fields. As observed, for those cases where our simulator could find a solution, there is a better agreement between the realizations and the reference image (solid curve) if FILTERSIM (dotted curves) or HOSIM (dash-dot curves) are used rather than when SGS (dashed curves) is employed. In Figures 23 and 24, the oil produced for each realization after 150 days and at the end of the injection of this chemical mixture (after 1000 days) is shown respectively. As seen, after 1000 days of ASP flooding, similar volume of oil is produced, regardless of the stochastic method used to generate the permeability scenarios. Nevertheless, after 150 days of flooding, important differences are observed. As discussed in Section 3.1 for the surfactant flooding, if SGS permeability fields are used, the oil recoveries are not accurately reproduced since the relative error of the oil recovery production with respect to the reference solution is around 21%. On the contrary, these are better captured with FILTERSIM and HOSIM permeability fields. As already commented for the surfactant flooding, weak variations when reproducing the high-permeability channels lead to lower oil variations.

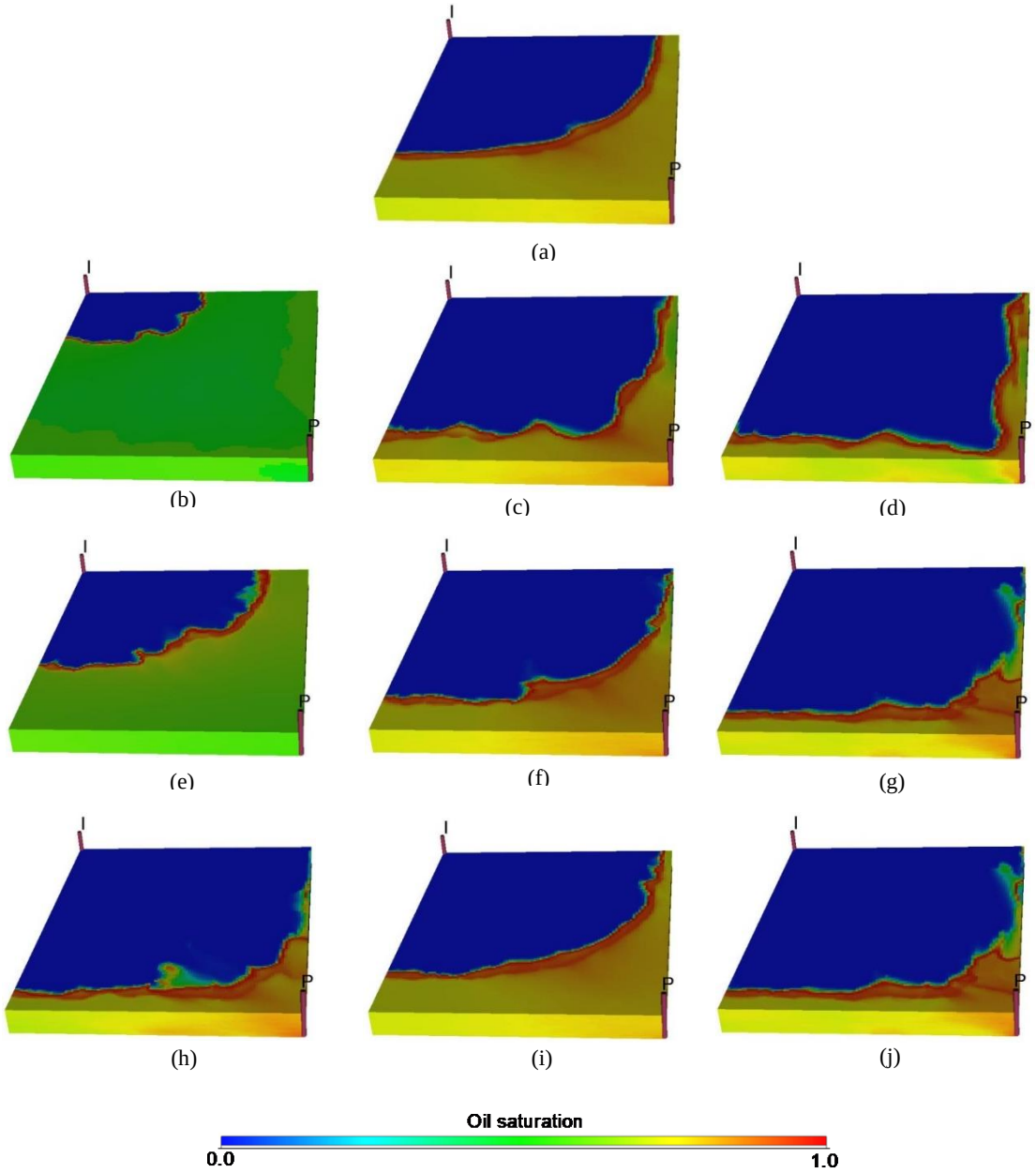

Figure 19: ASP flooding: oil saturation profiles at day 90 in case of the reference image (first row), SGS realizations (second row), FILTERSIM realizations (third row) and HOSIM realizations (fourth row). Note that in these last three rows, the oil saturation profiles corresponding to the lowest oil recovery (first column), a medium oil recovery (second column) and the highest low recovery (third column) have been selected.

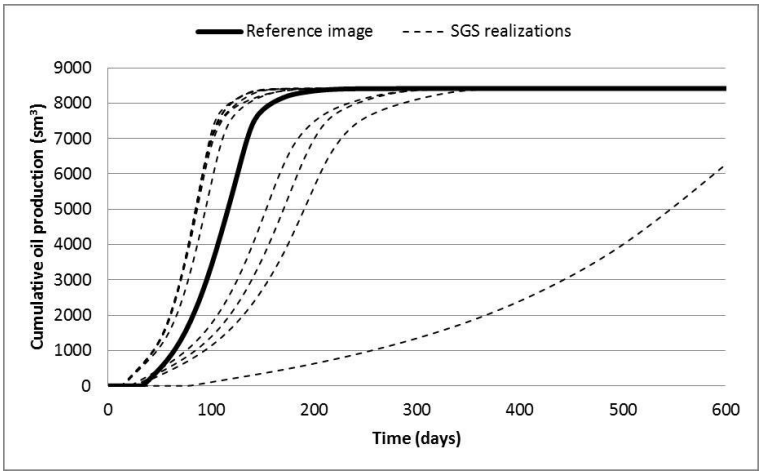

Figure 20: Oil production versus time curves for the reference image (solid line) and the SGS (dashed lines) realizations in case of ASP flooding.

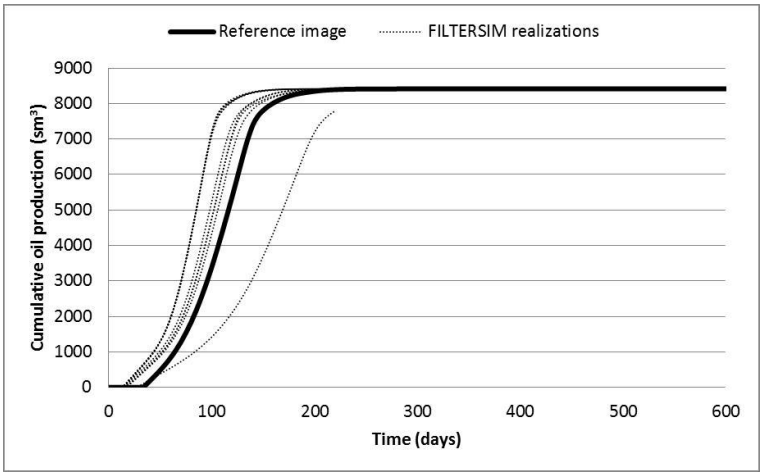

Figure 21: Oil production versus time curves for the reference image (solid line) and the FILTERSIM (dotted lines) realizations in case of ASP flooding.

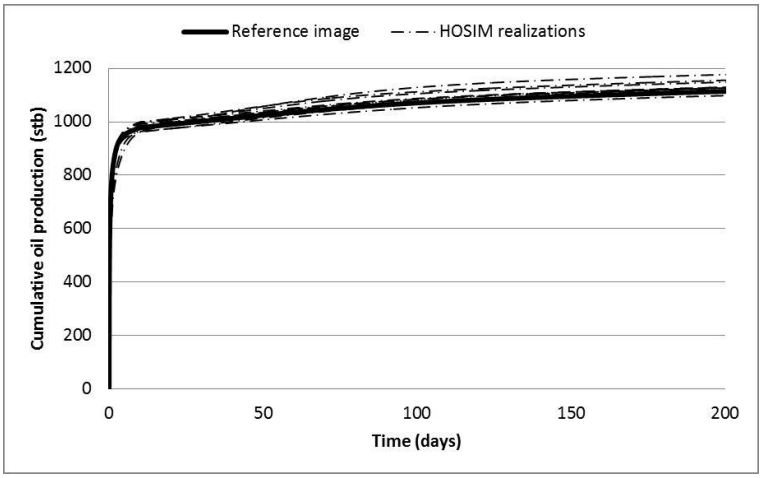

Figure 22: Oil production versus time curves for the reference image (solid line) and the HOSIM (dash-dot lines) realizations in case of ASP flooding.

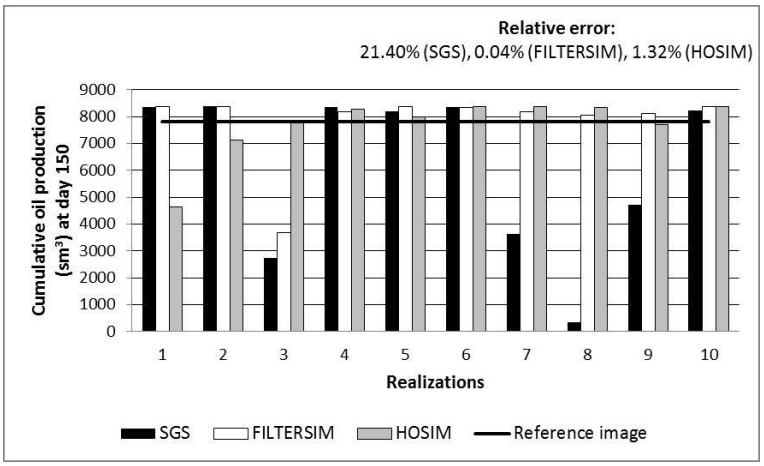

Figure 23: Cumulative oil production obtained for each realization after 150 days in case of ASP flooding.

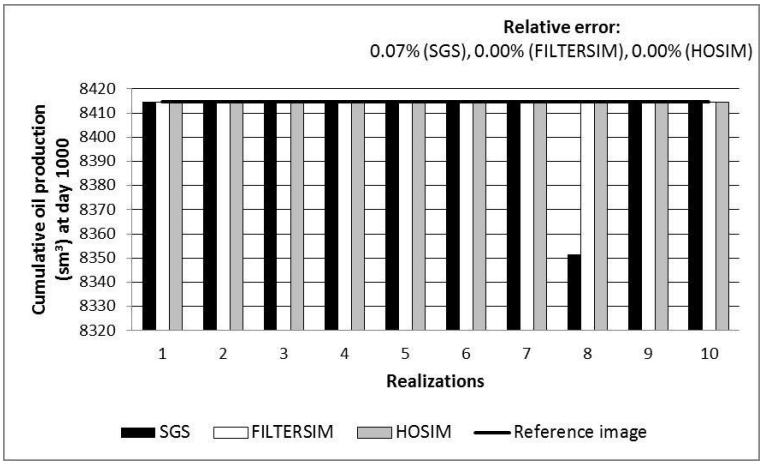

Figure 24: Cumulative oil production obtained for each realization after 1000 days in case of ASP flooding.

3.4 Foam flooding

As a fourth test, a foam flooding process is here considered, with the 3D domain (100 ft x 130 ft x 10 ft) of Figure 3. Note that here, field units have been considered. First, gas is injected for a period of 10 days. Then, for a period of 300 days, foam is added to the injected gas at a concentration of 30 lb/Mscf. The rate of injection during all the flooding process is such that the surface flow rate is 100000 Mscf/day.

The oil saturation profiles at day 1 are shown in Figure 25. The smooth propagation of the oil saturation profile obtained when the reference image is considered, see Figure 25(a), is not preserved if SGS and FILTERSIM realizations are employed, see Figures 25(b)-25(d) and Figures 25(e)-25(g) respectively. On the contrary, if the HOSIM algorithm is used to generate the different permeability scenarios, the flow behavior is more uniform and few differences are observed from one realization to another, as shown in Figures 25(h)-(j). Moreover, these oil saturation profiles are similar to the one obtained when the reference image is considered.

For the sake of comparison, the cumulative oil production of the first 200 days, see Figures 26 to 28, is here used again to analyze the impact of geologic heterogeneity. As seen, a good agreement from one realization to another and with respect to the reference image is obtained. In Figures 29 and 30, the oil produced for each realization after 50 days and at the end of the flow simulations (after 310 days) is displayed respectively. Compared to surfactant and ASP floodings, for those cases where our simulator could find a solution, geologic heterogeneity has little impact on oil recovery curves if foam flooding is employed: regardless of the stochastic method used to generate the permeability scenarios, the relative error of the oil recovery production with respect to the reference image is less than 3%.

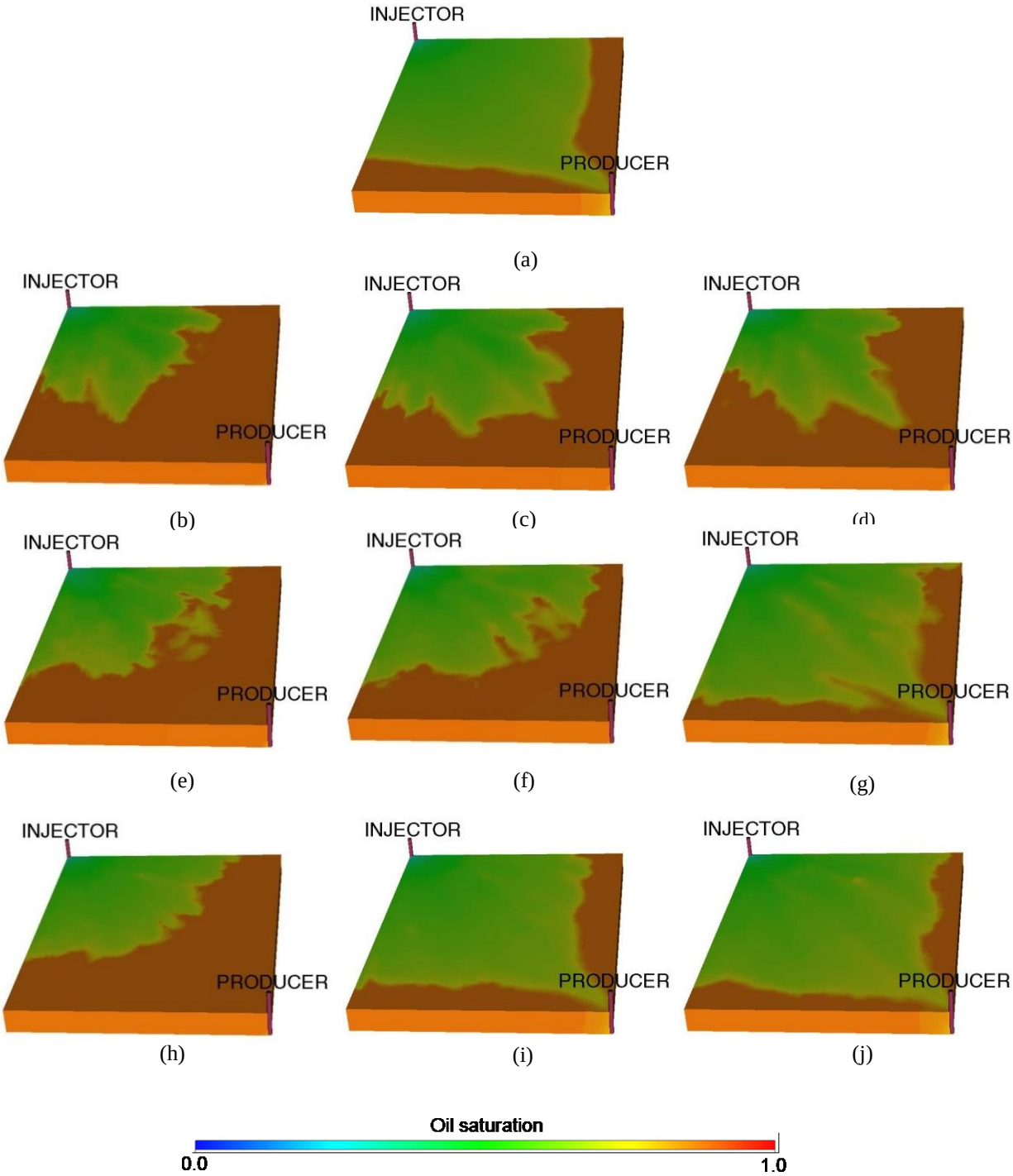

Figure 25: Foam flooding: oil saturation profiles at day 1 in case of the reference image (first row), SGS realizations (second row), FILTERSIM realizations (third row) and HOSIM realizations (fourth row). Note that in these last three rows, the oil saturation profiles corresponding to the lowest oil recovery (first column), a medium oil recovery (second column) and the highest low recovery (third column) have been selected.

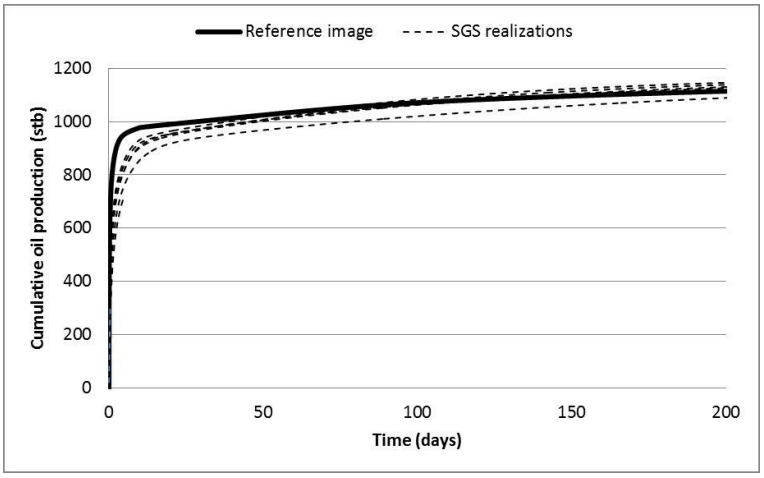

Figure 26: Oil production versus time curves for the reference image (solid line) and the SGS (dashed lines) realizations in case of foam flooding.

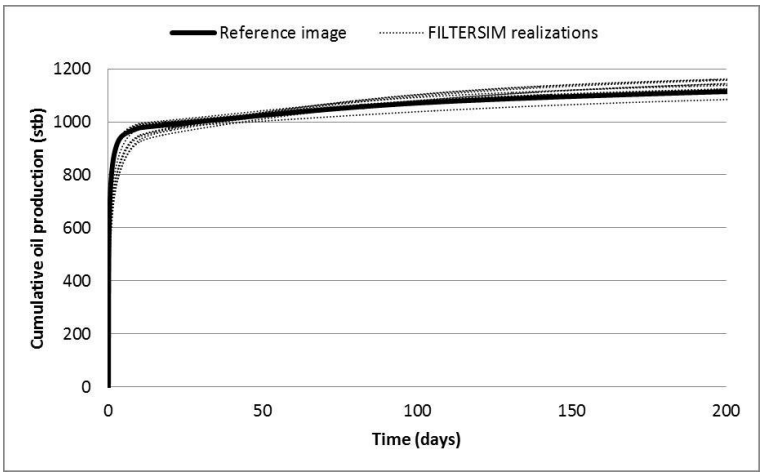

Figure 27: Oil production versus time curves for the reference image (solid line) and the FILTERSIM (dotted lines) realizations in case of foam flooding.

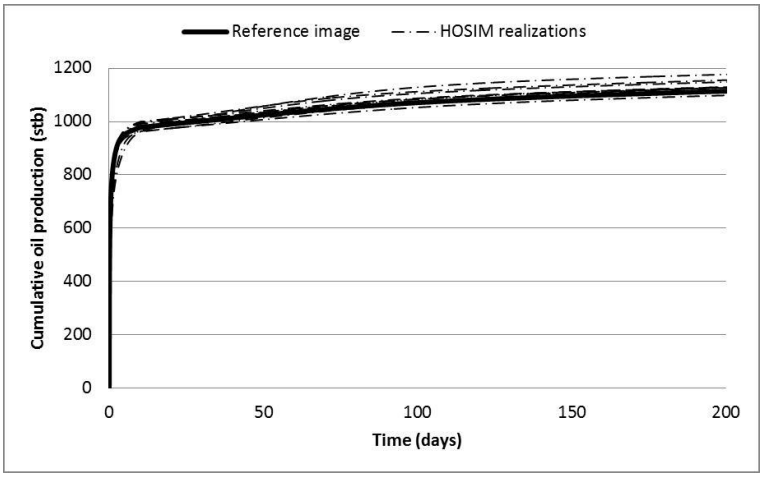

Figure 28: Oil production versus time curves for the reference image (solid line) and the HOSIM (dash-dot lines) realizations in case of foam flooding.

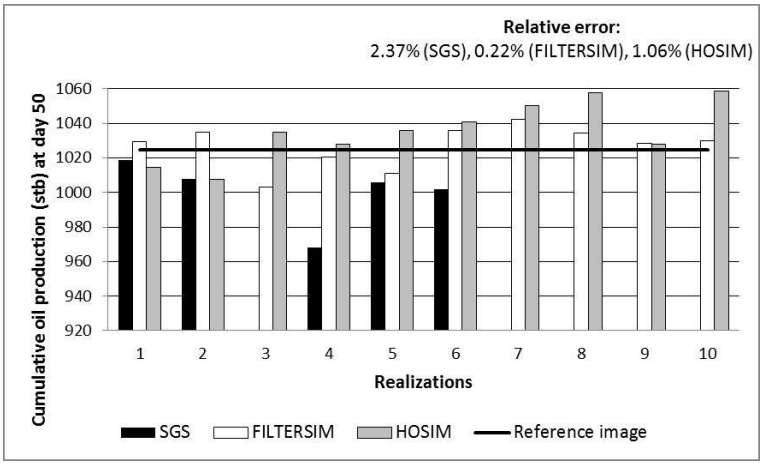

Figure 29: Cumulative oil production obtained for each realization after 50 days in case of foam flooding.

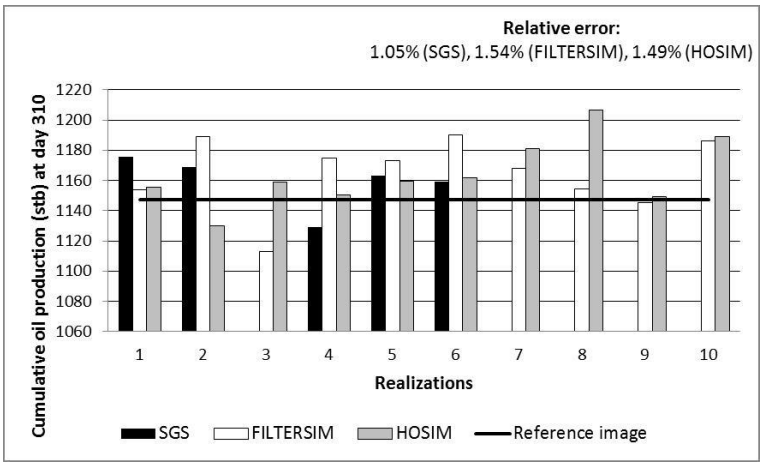

Figure 30: Cumulative oil production obtained for each realization after 310 days in case of foam flooding.

4 Conclusions

In this paper, the effect of different simulation algorithms utilized for the spatial distribution of the permeability field and consequent flow responses are tested and assessed, when EOR techniques are taken into account. The three different stochastic methods used to represent geological heterogeneity are: 1) the two-point method SGS, 2) the well-known multiple-point method FILTERSIM, and 3) a new alternative high-order simulation method that uses high-order spatial statistics (HOSIM). The results show that 1) the sequential Gaussian simulation algorithm suffers from the inability of reproducing curvilinear channels; 2) a more appropriate connectivity in the high-permeability values is obtained if the filter-based simulation method FILTERSIM is used, since this algorithm is not limited to two-point statistics but infers richer structural information from the reference image; and 3) a better agreement with the reference image of these curvilinear high-permeability channels is obtained if a data-driven high order algorithm is employed.

These methods have been compared by illustrating their effects on reservoir flow simulations when considering EOR techniques. The results presented show that the impact of geologic heterogeneity clearly depends on the flooding process under consideration:

Geologic heterogeneity has a major influence if surfactant or a mixture of alkaline, surfactant and polymer (ASP) is injected. In these two flooding processes, similar flow responses are obtained. On the one hand, the uniform propagation of the oil saturation profile is not observed if SGS realizations are used as permeability fields. FILTERSIM and HOSIM permeability scenarios lead to a more uniform propagation of oil. On the other hand, regarding the

cumulative oil, there is a better agreement between the realizations and the reference image if these two latter methods are used rather than when SGS is employed. With FILTERSIM and HOSIM realizations, the oil produced is less spread from its average whereas SGS realization span a wide range.

Geologic heterogeneity has little impact on oil recovery curves if foam is injected into the fluid stream: regardless of the geostatistical simulation algorithm used to generate the permeability scenarios, low relative standard deviations are obtained. Nevertheless, it does have an effect in the flow behavior: the smooth propagation of the oil saturation profile is only preserved if HOSIM realizations are employed as permeability fields.

Small differences in the flow behavior from one realization to another and with respect to the reference image are observed in case of polymer flooding: a very good agreement between all the obtained oil saturation profiles and the oil production versus time curves is observed, regardless of the stochastic method employed to generate the different permeability scenarios.

References

Alajmi, A.F., R.B. Gharbi and R. Chase (2010). The performance of polymer floods in partially fractured reservoirs. Journal of Porous Media 13(11), 961–971. doi: 10.1615/JPorMedia.v13.i11.20.

Alkhatib, A.M. (2014). Applying the Multi-level Monte Carlo Method to Quantify Uncertainty for Chemical EOR Processes. In Second EAGE Integrated Reservoir Modelling Conference. doi: 10.3997/2214-4609.20147448.

Alkhatib, A. and P. King (2014). Robust quantification of parametric uncertainty for surfactant–polymer flooding. Computational Geosciences 18(1), 77–101 . doi: 10.1007/s10596-013-9384-9.

AlSofi, A.M. and M.J. Blunt (2014). Polymer flooding design and optimization under economic uncertainty. Journal of Petroleum Science and Engineering 124, 46–59. doi: 10.1016/j.petrol.2014.10.014.

Alusta, G.A., E.J. Mackay, J. Fennema, K. Armih and I. Collins (2012). EOR vs. Infill Well Drilling: Sensitivity to Operational and Economic Parameters. In North Africa Technical Conference and Exhibition. Society of Petroleum Engineers. doi: http://dx.doi.org/10.2118/150454-MS.

Alvarado, V. and E. Manrique (2010). Enhanced Oil Recovery: An Update Review. Energies 3(9), 1529-1575. doi: 10.3390/en3091529.

Arpat, G.B. (2004). Sequential simulation with patterns. PhD Thesis, Stanford University.

Brown, C.E. and P.J. Smith (1984). The Evaluation of Uncertainty in Surfactant EOR Performance Prediction. In SPE Annual Technical Conference and Exhibition. Society of Petroleum Engineers. doi: http://dx.doi.org/10.2118/13237-MS.

Bu, T. and S.I. Aanonsen (1991). Surfactant flooding uncertainty analysis. In IOR 1991 – 6th European Symposium on Improved Oil Recovery. doi: 10.3997/2214-4609.201411207.

Carrero, E., N.V. Queipo, S. Pintos and L.E. Zerpa (2007). Global sensitivity analysis of Alkali–Surfactant–Polymer enhanced oil recovery processes. Journal of Petroleum Science and Engineering 58(1-2), 30–42. doi: 10.1016/j.petrol.2006.11.007.

Castor, T.P., W.H. Somerton and J.F. Kelly (1981). Recovery Mechanisms of Alkaline Flooding. In Surface Phenomena in Enhanced Oil Recovery, by D. O. (Ed.) Shah, 249–291. Springer US. doi: 10.1007/978-1-4757-0337-5_14.

Choudhary, M., B. Parekh, H. Solis, B. Meyer, K. Shepstone, E. Dezabala, C. Prostebby, E. Manrique, M. Izadi and D. Larsen (2014). Reservoir In-Depth Waterflood Conformance: An Offshore Pilot Implementation. In SPE Improved Oil Recovery Symposium. Society of Petroleum Engineers. doi: http://dx.doi.org/10.2118/169132-MS.

Comunian, A., P. Renard, and J. Straubhaar (2012). 3D multiple-point statistics simulation using 2D training images. Computers & Geosciences 40, 49–65. doi: 10.1016/j.cageo.2011.07.009.

Costa, A.P.A and D.J. Schiozer (2008). Use of Representative Models to improve the decision making process of chemical flooding in a mature field. In SPE Russian Oil and Gas Technical Conference and Exhibition. Society of Petroleum Engineers. doi: http://dx.doi.org/10.2118/115442-MS.

Dang, C.T.Q., L.X. Nghiem, Z. Chen, N.T.B. Nguyen and Q.P. Nguyen (2014). CO2 Low Salinity Water Alternating Gas: A New Promising Approach for Enhanced Oil Recovery. In SPE Improved Oil Recovery Symposium. Society of Petroleum Engineers. doi: http://dx.doi.org/10.2118/169071-MS.

Delshad, M., N.F. Najafabadi, G. Anderson, G.A. Pope and K. Sepehrnoori (2009). Modeling Wettability Alteration By Surfactants in Naturally Fractured Reservoirs. SPE Reservoir Evaluation & Engineering, 12(03), 361–370. doi: http://dx.doi.org/10.2118/100081-PA.

Deutsch, C.V. and A.G. Journel (1998). GSLIB: geostatistical software library and user's guide. New York: Oxford University Press.

Deutsch, C. V. and T. A. Hewett (1996). Challenges in reservoir forecasting. Mathematical Geology 28(7), 829–842. doi: 10.1007/BF02066003.

Dimitrakopoulos, R. and X. Luo (2004). Generalized Sequential Gaussian Simulation on Group Size v and Screen-Effect Approximations for Large Field Simulations. Mathematical Geology 36(5), 567–591. doi: 10.1023/B:MATG.0000037737.11615.df.

Dimitrakopoulos, R., H. Mustapha and E. Gloaguen (2010). High-order Statistics of Spatial Random Fields: Exploring Spatial Cumulants for Modeling Complex Non-Gaussian and Non-linear Phenomena. Mathematical Geosciences 42(1), 65–99. doi: 10.1007/s11004-009-9258-9.

Fisher, A.W., R.W.S. Foulser and S.G. Goodyear (1990). Mathematical Modeling of Foam Flooding. In SPE/DOE Enhanced Oil Recovery Symposium. Society of Petroleum Engineers. doi: http://dx.doi.org/10.2118/20195-MS.

Galard, D. Lefebvre, C., S. Serbutoviez, D. Sorin (2012). Building a Roadmap for Enhanced Oil Recovery Prefeasibility Study. In SPE Russian Oil and Gas Exploration and Production Technical Conference and Exhibition. Society of Petroleum Engineers. doi: http://dx.doi.org/10.2118/159264-MS.

Ghori, S.G., A. Ouenes, G.A. Pope, K. Sepehrnoori and J.P. Heller (1992). The Effect of Four Geostatistical Methods on Reservoir Description and Flow Mechanism. In SPE Annual Technical Conference and Exhibition. Society of Petroleum Engineers. doi: http://dx.doi.org/10.2118/24755-MS.

Gittler, W.E. and P.H. Krumrine (1985). A Novel Approach for Risk Assessment in Chemical EOR Projects. In SPE Hydrocarbon Economics and Evaluation Symposium. Society of Petroleum Engineers. doi: http://dx.doi.org/10.2118/13767-MS.

Goovaerts, P (1997). Geostatistics for natural resources evaluation. New York: Oxford university press.

Guardiano, F.B. and R.M. Srivastava (1993). Multivariate Geostatistics: Beyond Bivariate Moments. Vol. 5, in Geostatistics Tróia '92, edited by Amilcar Soares, 133–144. Springer Netherlands. doi: 10.1007/978-94-011-1739-5_12.

Honarkhah, M. and J. Caers (2012). Direct pattern-based simulation of non-stationary geostatistical models. Mathematical Geosciences 44(6), 651–672. doi: 10.1007/s11004-012-9413-6.

Hu, L.Y. and T. Chugunova (2008). Multiple-point geostatistics for modeling subsurface heterogeneity: A comprehensive review. Water Resources Research 44(11), W11413. doi: 10.1029/2008WR006993.

IEA (2013). Resources to Reserves 2013 Oil, Gas and Coal Technologies for the Energy Markets of the Future. International Energy Agency. doi: 10.1787/9789264090705-en.

Journel, A.G. (1989). Fundamentals of Geostatistics in Five Lessons. Short Course in Geology. American Geophysical Union, Washington DC.

Journel, A.G. (1994). Modeling Uncertainty: Some Conceptual Thoughts. In Dimitrakopoulos, R. (Ed.), Geostatistics for the Next Century. Vol. 6 of Quantitative Geology and Geostatistics. Springer Netherlands, 30–43. doi: 10.1007/978-94-011-0824-9_5.

Journel, A.G. and F.G. Alabert (1988). Focusing on spatial connectivity of extreme-valued attributes: stochastic indicator models of reservoir heterogeneities. In SPE Annual Technical Conference & Exhibiton Volume SIGMA. Society of Petroleum Engineers of AIME (Paper) SPE, 621–632.

Kianinejada, A., M.H. Ghazanfaria, R. Kharratb and D. Rashtchian (2013). An Experimental Investigation of Surfactant Flooding as a Good Candidate for Enhancing Oil Recovery from Fractured Reservoirs Using One-Quarter Five Spot Micromodels: The Role of Fracture Geometrical Properties. Energy Sources, Part A: Recovery, Utilization, and Environmental Effects 35(20), 1929–1938. doi: 10.1080/15567036.2010.525591.

Langtangen, H.P. (1991) Sensitivity analysis of an enhanced oil recovery process. Applied Mathematical Modelling 15(9), 467–474. doi: 10.1016/0307-904X(91)90036-O.

Mantilla, C.A. and S. Srinivasan (2011). Feedback control of polymer flooding process considering geologic uncertainty. In SPE Reservoir Simulation Symposium. Society of Petroleum Engineers. doi: http://dx.doi.org/10.2118/141962-MS.

Mao, S. and A. Journel (1999). Generation of a reference petrophysical and seismic 3D data set, The Stanford V reservoir. Stanford Center for Reservoir Forecasting Annual Meeting, SCRF Report, Stanford University.

Mariethoz, G. and S. Lefebvre (2014). Bridges between multiple-point geostatistics and texture synthesis: Review and guidelines for future research. Computers and Geosciences 66, 66–80. doi: 10.1016/j.cageo.2014.01.001.

Mollaei, A., L.W. Lake and M. Delshad (2011). Application and variance based sensitivity analysis of surfactant–polymer flooding using modified chemical flood predictive model. Journal of Petroleum Science and Engineering 79(1-2), 25–36. doi: 10.1016/j.petrol.2011.07.016.

Muggeridge, A., A. Cockin, K. Webb, H. Frampton, I. Collins, T. Moulds and P. Salino (2014). Recovery rates, enhanced oil recovery and technological limits. Philosophical transactions of the royal society A: Mathematical, Physical and Engineering Sciences, 372(2006), 20120320. doi: 10.1098/rsta.2012.0320.

Mustapha, H., S. Chatterjee and R. Dimitrakopoulos (2014). CDFSIM: Efficient Stochastic Simulation Through Decomposition of Cumulative Distribution Functions of Transformed Spatial Patterns. Mathematical Geosciences 46(1), 95–123. doi: 10.1007/s11004-013-9490-1.

Mustapha, H. and R. Dimitrakopoulos (2011). HOSIM: A high-order stochastic simulation algorithm for generating three-dimensional complex geological patterns. Computers & Geosciences 37(9), 1242–1253. doi: 10.1016/j.cageo.2010.09.007.

Mustapha, H. and R. Dimitrakopoulos (2010). A new approach for geological pattern recognition using high-order spatial cumulants. Computers & Geosciences 36(3), 313–334. doi: 10.1016/j.cageo.2009.04.015.

Nguyen, N.T.B., Z.J. Chen, L.X. Nghiem, C.T.Q. Dang and C. Yang (2014). A New Approach for Optimization and Uncertainty Assessment of Surfactant-Polymer Flooding. In Abu Dhabi International Petroleum Exhibition and Conference. Society of Petroleum Engineers. doi: http://dx.doi.org/10.2118/172003-MS.

Othman, M.B., S. Jalan, R. Masoudi and M. S. M. Shaharudin (2013). Chemical EOR: Challenges for Full Field Simulation. In SPE Enhanced Oil Recovery Conference . Society of Petroleum Engineers. doi: http://dx.doi.org/10.2118/165247-MS.

Pyrcz, M.J. and C.V. Deutsch (2014). Geostatistical Reservoir Modeling. Edited by Oxford university press.

Remy, N., A. Boucher and J. Wu (2009). Applied geostatistics with SGeMS: a user's guide. Cambridge University Press.

Sandrea, I. and R. Sandrea (2007). Global Oil Reserves-1: Recovery factors leave vast target for EOR technologies. Oil and Gas Journal 105(41), 44–47.

Schlumberger (2014). Eclipse Technical Description.

Schramm, L.L. (2000). Surfactants: fundamentals and applications in the petroleum industry. Cambridge University Press.

Shah, D. O. (2012). Improved oil recovery by surfactant and polymer flooding. Elsevier.

Straubhaar, J., P. Renard, G. Mariethoz, R. Froidevaux and O. Besson (2011). An Improved Parallel Multiple-point Algorithm Using a List Approach. Mathematical Geosciences 43(3), 305–328. doi: 10.1007/s11004-011-9328-7.

Strebelle, S. (2002). Conditional Simulation of Complex Geological Structures Using Multiple-Point Statistics. Mathematical Geology 34(1), 1–21. doi: 10.1023/A:1014009426274.

Strebelle, S., and C. Cavelius (2014). Solving speed and memory issues in multiple-point statistics simulation program SNESIM. Mathematical Geosciences 46(2), 171–186. doi: 10.1007/s11004-013-9489-7.

Wu, J., A. Boucher and T. Zhang (2008). A SGeMS code for pattern simulation of continuous and categorical variables: FILTERSIM. Computers & Geosciences 34(12), 1863–1876. doi: 10.1016/j.cageo.2007.08.008.

Yu, K.W., B.I. Choi and K.S. Lee (2013). Assessment of NPV Uncertainty on Heterogeneous Reservoirs during Polymer Flood. Applied Mechanics and Materials 448-453, 4033–4037. doi: 10.4028/www.scientific.net/AMM.448-453.4033.

Zhang, T., P. Switzer and A. Journel (2006). Filter-Based Classification of Training Image Patterns for Spatial Simulation. Mathematical Geology 38(1), 63–80. doi: 10.1007/s11004-005-9004-x.